Published in final edited form as:

Mol Cancer Res. 2019 April ; 17(4): 907–917. doi:10.1158/1541-7786.MCR-18-0931.

Unraveling the Cellular Mechanism of Assembling Cholesterols for Selective Cancer Cell Death

Huaimin Wang[1], **Zhaoqianqi Feng**[1], **Cuihong Yang**[2], **Jinjian Liu**[2], **Jamie E. Medina**[3], **S. Ali Aghvami**[4], **Daniela M. Dinulescu**[3], **Jianfeng Liu**[2], **Seth Fraden**[4], and **Bing Xu**[1]

[1]Department of Chemistry, Brandeis University, 415 South Street, Waltham, MA 02454, USA

[2]Chinese Academy of Medical Science & Peking Union Medical College, Tianjin 300192, China

[3]Department of Pathology, Brigham and Women's Hospital, Harvard Medical School, Boston, MA 02115 (USA)

[4]Department of Physics, Brandeis University, 415 South Street, Waltham, MA 02454, USA

Abstract

Acquired drug resistance remains a challenge in chemotherapy. Here we show enzymatic, in-situ assembling of cholesterol derivatives to act as polypharmaceuticals for selectively inducing death of cancer cells *via* multiple pathways and without inducing acquired drug resistance. A conjugate of tyrosine and cholesterol (**TC**), formed by enzyme catalyzed dephosphorylation of phosphorylate TC (**pTC**), self-assembles selectively on or in cancer cells. Acting as polypharmaceuticals, the assemblies of TC augment lipid rafts, aggregate extrinsic cell death receptors (e.g., DR5, CD95, or TRAILR), modulate the expression of oncoproteins (e.g., Src and Akt), disrupt the dynamics of cytoskeletons (e.g., actin filaments or microtubules), induce ER stress, and increase the production of reactive oxygen species (ROS), thus resulting in cell death and preventing acquired drug resistance. Moreover, the assemblies inhibit the growth of platinum-resistant ovarian cancer tumor in a murine model. This work illustrates the use of instructed-assembly (iA) in cellular environment to form polypharmaceuticals in-situ that not only interact with multiple proteins, but also modulate membrane dynamics for developing novel anticancer therapeutics.

Corresponding Author: Bing Xu, Department of Chemistry, Brandeis University, 415 South Street, Waltham, MA 02454, USA. bxu@brandeis.edu.

Authors' Contributions

Conception and design: H. Wang, B. Xu

Development of methodology: H. Wang, Z. Feng, B. Xu

Acquisition of data (provided animals, acquired and managed patients, provided facilities, etc.): H. Wang, Z. Feng, C. Yang, J. Liu, J. Medina, S. Aghvami, D. Dinulescu, J. Liu, S. Fraden, B. Xu

Analysis and interpretation of data (e.g., statistical analysis, biostatistics, computational analysis): H. Wang, B. Xu

Writing, review, and/or revision of the manuscript: H. Wang, Z. Feng, B. Xu

Administrative, technical, or material support (i.e., reporting or organizing data, constructing databases): B. Xu

Study supervision: B. Xu

Disclosure of Potential Conflicts of Interest

No potential conflicts of interest were disclosed.

Keywords

self-assembly; cholesterol; anticancer; drug-resistance; ER stress

Introduction

Tumor cells differ remarkably from their normal cell counterpart due to the longtime oncogenic mutation. The advances of high-throughput sequencing reveal that tumorigenesis mutations are more numerous and heterogeneous than previously thought.(1,2) Moreover, according to detailed bioinformatics analyses,(3) cancer related driver mutations influence a dozen or more core signaling pathways and processes that are responsible for tumorigenesis. These findings raised the questions about the usefulness of targeting individual signaling molecules as a practical therapeutic strategy. To date, various synthetic and natural derived anticancer drugs, with different or similar modes of actions, have entered clinical cancer therapy.(4) The problem of selectivity and acquired drug resistance, however, remain a challenge. Despite the exciting development of immunotherapy, many cancers still are unresponsive to immunotherapy.(5) Thus, there is a need of novel strategy for combating cancers. An emerging concept to address that need is polypharmacology, which aims to develop multitarget drugs,(6) that is, a therapeutic agent that interacts with more than one target or carries out more than one functions. In fact, it is rather common for endogenous molecules, small bioactive molecules or macromolecules, to exhibit multiple functions that are context dependent. One of most notable multifunctional small molecules is cholesterol, which plays an indispensable roles in modulating cell signaling transduction and maintain cell membrane hemostasis in mammalian cells.(7) The dynamic clustering of cholesterol and sphingolipids form raft like structures, which function as a platform for tuning the dynamics of membrane proteins and signal transduction.(8) Recent studies also unveiled important approaches that target plasma membrane for modulating immune cell signaling to enhance immune response against cancer cells.(9) These advancements support the exploration of therapeutics outside the domain of tight ligand-receptor or antibody-antigen interactions.

To explore outside the dogma of ligand receptor binding, we have been developing instructed-assembly (iA) of small molecules for generating higher order structures in cellular environment, which exhibits exciting promises in cancer therapy or imaging.(10–12) Our recent finding revealed that pericellular assemblies instructed by GPI anchored ectoenzymes (e.g., alkaline phosphatases(13)) on cell membrane selectively induce cancer cell death.(14) To reduce the dosage for satisfying clinical needs, we developed a cholesterol derivative (**pTC-1**) as the molecules for iA. Our results indicate that **pTC-1** exhibits excellent potency against platinum resistant ovarian cancer cells.(15) Previous results of solid NMR indicated that **pTC-1** transformed to **TC-1** in the presence of phosphatase. We also have found that uncompetitive inhibitors of phosphatase in cells rescue cells from exposure to **pTC-1**, and dephosphorylation of **pTC-1** by exogenous ALP abolish the cytotoxicity of **pTC-1**.(15) These results together suggested the importance of iA for inducing cell death. The precise cellular mechanism of the selective cancer cell death resulted from the iA of **pTC-1**, however, remains to be elucidated, and the in vivo efficacy of iA of **pTC-1** has yet to be examined.

In this work, using various biochemical methods, we show that enzymatically-controlled, in-situ assemblies of the cholesterol derivative acts as polypharmaceuticals for selectively inducing death of cancer cells *via* multiple death pathways and without resulting in acquired drug resistance. Specifically, **pTC-1** is able to form assemblies of **TC-1** (after dephosphorylation) selectively on or in cancer cells (Scheme 1). The assemblies of **TC-1** augment lipid rafts, aggregate extrinsic cell death receptors (e.g., DR5, CD95 or TRAILR), decrease the expression of oncoproteins (e.g., Src and Akt), disrupt the dynamics of cytoskeletons (e.g., actin filaments or microtubules), induce endoplasmic reticulum (ER) stress, and increase the production of reactive oxygen species (ROS), thus resulting in cell death and minimizing acquired drug resistance. Moreover, xenograft mouse model demonstrates that intraperitoneal injection of **pTC-1** inhibits the growth of the tumor of platinum-resistant ovarian cancer, confirming that iA of **pTC-1** is effective *in vivo*. This study illustrates a new approach for designing iA that utilizes essential, endogenous enzymes to spatiotemporally modulate membranes and proteins for multi-targeting and regulating cell behavior, which promises a potential approach to advance anticancer nanomedicines, overcome cancer drug resistance, and complement with immunotherapy.

Materials and Methods

Reagents

HeLa, Saos-2, HS-5, HepG2, T98G, and A2780 cells were purchased from American-type Culture Collection (ATCC, USA), A2780cis cell from Sigma, and Kuramochi and OVSAHO cell lines from the lab of Dinulescu lab at Harvard Medical School. Dulbecco's modified Eagle's medium (DMEM), McCoy's 5a medium, and 1640 Medium were purchased from ATCC, and fetal bovine serum (FBS) and penicillin/streptomycin from Gibco by Life Technologies. 3-(4,5-Dimethylthiazol-2-yl)-2,5-diphenyltetrazolium bromide (MTT) was purchased from ACROS Organics, ER stress antibody kit from Cell Signaling Technology, and other antibodies from Abcam.

Cell culture

HeLa, T98G, HepG-2, HS-5 and Saos-2 cell lines were purchased from ATCC between 2010 and 2017. A2780cis cells were obtained from Sigma-aldrich in 2016. Kuramochi and OVSAHO were kindly provided by Prof. Dinulescu (Harvard medical school). All cell lines were authenticated using short tandem repeat DNA fingerprinting. A2780cis cells were cultured in RPMI 1640 medium supplemented with 10% v/v fetal bovine serum, 100 U/mL penicillin, and 100 μg/mL streptomycin (cisplatin only necessary every 2–3 passages). HeLa cells, T98G, and HepG-2 cells were cultured in MEM medium supplemented with 10% v/v fetal bovine serum, 100 U/mL penicillin and 100 μg/mL streptomycin; HS-5 cells were cultured in Dulbecco's Modified Eagle's medium (DMEM) supplemented with 10% v fetal bovine serum (FBS), 100 U/mL penicillin, and 100 μg/mL streptomycin; Saos-2 cells were cultured in McCoy's 5a medium (for Saos-2) supplemented with 15% v/v fetal bovine serum, 100 U/mL penicillin, and 100 μg/mL streptomycin; Kuramochi and OVSAHO cell lines were cultured in RPMI-1640 medium with 10% FBS and 1% P/S. All cells were incubated at 37 °C in a humidified atmosphere of 5% CO_2.

MTT assay

All different cell lines were seeded in 96-well plates at 1×10^5 cells/well for 24 h followed by culture medium removal and subsequently addition of culture medium containing different amounts of the precursors. At designated time (24/48/72 h), we added 10 μL MTT solution (5 mg/mL) to each well and incubated at 37°C for another 4 h, and then 100 μL of SDS-HCl solution was added to stop the reduction reaction and to dissolve the purple formazan. The absorbance of each well at 595 nm was measured by a multimode microplate reader. The cytotoxicity assay was performed three times, and the average value of the three measurements was taken.

Actin Staining

Cells in exponential growth phase were seeded in a confocal dish (3.5 cm) at 1.5×10^5 cells per dish and allowed to fully attach to the culture dish bottom. After removing the culture medium, we added fresh medium containing the test compound. At designated time, we removed the medium and washed by PBS for three times, fixed by 4% paraformaldehyde for 15 minutes, and then added 1 mL of 0.1% Triton X-100 in PBS buffer for 30 minutes. After washing the cells three times by PBS, we added 1 mL of 0.1% BSA in PBS for 30 minutes, and then washed the cells by PBS for three times. 1 mL of PBS containing 5 unit of Alexa 633 was added to the cells for 1 h. After removing the buffer and washing the cells three times by PBS, we added 1 mL of Hoechst (1 μg/mL) for 10 minutes. Then, the cells were washed three times with PBS buffer before imaging.

Time dependent Western blot

Cells in exponential growth phase were seeded in 10 cm culture dish and allowed to fully attach to the culture dish bottom. Upon 70% to 80% confluences, we treated cells with the different compounds at different concentrations for time range from 0 to 24 h. After the cells were washed by cold PBS buffer for five times, we added cell lysis buffer to the plate for 5 minutes, and then cells were scraped. The lysate solution was transferred into a 1.5 mL Appendorf. After centrifuged the sample for 20 minutes at 12,000x g in a cold microfuge, the supernatant was collected for quantifying the protein concentration by Pierce™ Coomassie Plus (Bradford) Assay Kit. 20 μL loading sample with SDS loading buffer was added in each lane for SDS-PAGE and Western blot analysis. After boiling the loading samples at 100 °C for 5 minutes, equal amounts of loading sample (20 μL) were separated using sodium dodecyl sulfate–polyacrylamide gel electrophoresis (SDS-PAGE) in TGS buffer and transferred to PVDF membranes. After blocking with TBST (TBS with 0.1% Tween 20) containing 5 % Bovine Serum Albumin (BSA) for 1 h, the membranes were incubated with the primary antibodies at 4 °C in TBST buffer that containing 5% BSA overnight. After washing the membrane for five times by TBST, we incubated the membrane with horseradish peroxidase (HRP)-conjugated goat anti-rabbit IgG antibodies in TBST buffer for 1 h at room temperature. After washing with TBST for 5 times, the blots were visualized with the Peirce ECL plus western blotting substrate.

In Vivo Evaluation of Antitumor Activity

All studies involving animals were approved by The Animal Care and Use Committee of IRM-CAMS. Female Balb/c mice were inoculated with 2×10^5 A2780cis cells in the mammary fat pad. Tumor growth was monitored every other day. Tumor volume was calculated by the formula: length×width×(Length+Width)/2. After tumors size reached ~50 mm^3, mice were randomly divided into different treatment groups (n = 6). The day giving compound was designated as day 0 and the compound was given in every two days. Mice weight was monitored after receiving treatment and presented as relative weight (%).

Results

Inhibition of multiple cancer cell lines

Acquired drug resistance is a major reason that makes chemotherapy ineffective. Our previous results indicate that **pTC-1** (Figure 1A) inhibits the growth of cisplatin-resistant human ovarian cancer cell lines (A2780cis). We also confirmed that **pTC-1** selectively inhibit ovarian cancer cells over normal cells.(15) To evaluate whether **pTC-1** induces acquired resistance, we used the parent, cisplatin-sensitive A2780 cell line to incubate with **pTC-1** by gradually increasing concentrations of **pTC-1**, similar to the method used to induce cisplatin resistant ovarian cancer cell lines.(16) As a control, we also cultured A2780 cell lines with cisplatin. After the treatment of A2780 cell lines by **pTC-1** (or cisplatin) for five weeks, we tested these stimulated A2780 cells with **pTC-1** or cisplatin by MTT assay. As shown in Figure 1B (and Figure S1), the IC_{50} of **pTC-1** against A2780 cells (after five weeks stimulation of **pTC-1**) is 8.1 μM for 48 h, which is similar with the cytotoxicity of the **pTC-1** on the unstimulated A2780 cells (10.5 μM). On the contrary, the IC_{50} of cisplatin is more than 100 μM against A2780 cells (after five weeks stimulation of cisplatin), which is much higher than the IC_{50} of cisplatin against unstimulated A2780 cells (29.3 μM).

We next examined the effects of **pTC-1** on the viability of cultured cancer cells and normal cells (Figure 1C and S2). **pTC-1** treatment markedly induces cell death in ovarian cancer cells, including two high-grade serous ovarian cancer (HGSC) cell lines, Kuramochi cells and OVSAHO cells. The IC_{50} is 22 μM for Kuramochi cells and 27 μM for OVSAHO cells, which is about two times higher than its IC_{50} values against cisplatin-sensitive A2780 cells (10.5 μM) and cisplatin-resistant A2780cis cells (13 μM). After being incubated with adenocarcinoma (HeLa), **pTC-1** exhibits IC_{50} of 19 μM, which is comparable to its IC_{50} against ovarian cancer cells. In contrast, **pTC-1** shows less efficacy against human bone marrow stromal cells (HS-5, IC_{50} is 32 μM) and human osteosarcoma cancer cells (Saos-2, 40.7 μM), respectively. In addition, the incubation of **pTC-1** with hepatocellular carcinoma cells (HepG2) and glioblastoma cancer cells (T98G) results in the IC_{50} values at 45 and 48 μM, respectively. The cholesterol contents or cholesteryl ester contents of different cells (Figure 1C) hardly correlate with the cytotoxicity of **pTC-1** on different cell types, further indicating that the cell death induced by **pTC-1** is rather resulted from the process of iA than depends on the amount of cholesterol in different types of cells.

Disturbing actin dynamics and mitochondrial fusion and fission

An autophagy inhibitor, methyladenine (2 or 5 mM), hardly rescued both A2780cis and HeLa cells that treated with **pTC-1** (Figure S3), indicating that the cell death induced by **pTC-1** unlikely involved autophagy. Moreover, Annexin V-FITC Apoptosis/PI staining suggested that most of cells treated by **pTC-1** are early apoptotic cells, which shows fluorescence, few of the cells are necrotic cells (Figure S4). Actin filaments, as part of cytoskeleton, are critical for variety of cellular processes, including cell growth, division, motility, as well as apoptosis. Previously, we found that in-situ self-assembly of small molecules on cell surface led to disruption of actin filaments.(14,15) Being treated with **NBD-pTC-1**, an analogue of **pTC-1**, A2780cis and HeLa cells exhibited bright fluorescent on cell surface and some fluorescent puncta inside cytoplasm (Figure S5) after 1 h incubation the cells with the probes. In addition, more fluorescence appeared inside cells after 5 h incubation. These results confirm that the enzymatic assemblies form on the cell surface and in the cells. To gain more insights into the dynamics of globular and filamentous actin equilibrium in the presence of **pTC-1**, we used Alexa Fluor 633 Phalloidin to stain actin filament of A2780cis or HeLa cells that were incubated with **pTC-1** for different durations. We chose A2780 cells to examine the acquired drug resistance of **pTC-1** (with cisplatin as the reference). We chose HeLa cells since it is a cell line that has served as a model of human cell biology for decades. As shown in figure 2A, with the increase of incubation time, the actin filaments start to shrink and become much shorter after the treatment of **pTC-1** in both A2780cis and HeLa cells. Without the addition of **pTC-1**, actin filaments in A2780cis cells exhibit long and fibrous structures and high density at the cell boundary. In contrast, after the cells being incubated with **pTC-1** for 7 h, actin filaments in the cells exist as short fibers or aggregates. After being incubated with **pTC-1** for 12 h, the cells produce more short aggregates of actin filaments. The brighter fluorescence originated from the staining of actin filaments at the cell boundary becomes weaker, and the sizes of the cells start to shrink. 24 h after the treatment of **pTC-1**, there are only irregular, short, and dot-like structures of actin aggregates. The change of actin filaments in HeLa cells slightly differs from that in A2780cis cells. The actin filaments at the boundary of cells become denser, and the inner actin filaments become shorter after the treatment of **pTC-1** for 7 h. With the increase of time, actin filaments appear as dots (12 h) and the cells shrink. This phenomenon lasts for 24 h, accompanying by some of cells to exhibit apoptotic morphology.

Mutation in actin or actin binding proteins can influence apoptotic pathways in mitochondria, as revealed by recent reports.(17,18) Chen and co-workers demonstrated that mitochondrial dysfunctions induced by ALA-PDT results in reorganization of cytoskeleton, alternating cellular morphology and cellular adhesion.(18) These findings together indicate that the interaction between actin and mitochondria contribute cell death. Moreover, fragmented mitochondria is one of the early sign of activation of apoptosis.(19) Based on these facts and the influences of **pTC-1** on cytoskeleton, we examine how the iA of **pTC-1** affects the morphology of mitochondria. Using a cell line of which has a mitochondria protein (Cytochrome c (Cyt c) tagged by green fluorescent protein (GFP),(20) we monitored the changes of mitochondria during the early stage of cell death after the treatment of **pTC-1**. After the cells being incubated with **pTC-1** for 22 h, typical tubular mitochondrial structure of healthy cells (Figure 2C) disintegrates into small, spherical organelles (Figure

2D), suggesting that **pTC-1** results in fragmental mitochondria. To further investigate the contribution of iA of **pTC-1**, we also examined the effect of methyl-β-cyclodextrin (M-βCD) and U18666A on the viability of the cells incubated with **pTC-1**. The former disrupts lipid rafts by removing cholesterol from membranes, and the latter is a well-known intracellular cholesterol transport inhibitor.(21) As shown in figure 2E and F (Figure S6), M-βCD significantly protect the cells, rescuing both A2780cis and HeLa cells at high concentration of **pTC-1**. In contrast, U18666A slightly increases the viability of the A2780cis cells, but exhibit little protective effect on the HeLa cells, suggesting that the iA of **pTC-1** plays a critical role for inducing the cell death.

Cell death involves extrinsic death pathways

To determine the signaling pathways that involved in **pTC-1** caused cell death, we first determined the effects of **pTC-1** on extrinsic death pathways, which play important roles in various biological processes.(22) Time dependent Western blot analysis (Figure 3 A, C and S7) indicates that continuous incubation with **pTC-1** induces the increase of the expression levels of CD95, DR3, and DR5 in A2780cis cell lines, while the expression levels of TNF-R1 and DR4 remain almost constant with the treatment of **pTC-1** within 24 h. The changes of these death receptors slightly differ in HeLa cells (Figure 3B, D and S7), which express higher levels of DR3 and DR5. Two major bands of CD95 in A2780cis cells represent two forms of CD95, likely due to posttranslational modifications that are ubiquitous in mammalian cells.(23)

We also used immunofluorescence to investigate the changes of other extrinsic death receptors after the treatment of **pTC-1**. As shown in figure 3E, the treatment of **pTC-1** increases the expression levels of CD95, TNF-R1, and DR5. This observation is consistent with the results of Western blot. Notably, immunofluorescence indicates that DR5 co-localizes with the Golgi marker RCAS1 (Figure S8) and exhibits weak fluorescence on cell surface or other organelles, indicating that the activation of DR5 is ligand-independent intracellular activation.(24)

ER stress for cell death

Recent finding has suggested that up-regulation of DR5, as the critical step for ER stress, induces death of several human cancer cells after the treatment of thapsigargin.(25,26) Ashkenazi and co-workers also reported that DR5 integrates opposing unfolded protein response (UPR) signals to control ER-stress induced apoptosis.(24,27) Moreover, ER is the harbor of cholesterol, which traffics from late endosomes. The overburden of cholesterol accumulation in the ER likely contributes to macrophage apoptosis.(28) Inspiring from these work and considering that **pTC-1** induces expression of DR5 during cell death, we evaluated the change of major ER stress markers in both A2780cis and HeLa cells incubated with **pTC-1**. Time dependent Western blot shows that the expression levels of Chop, Bip, and PDI, the indictors of cells under ER stress, increase after the treatment of **pTC-1**, indicating the induction of ER stress. In addition, our results indicate that **pTC-1** induced ER stress also activates IRE1α branch of UPR, which is the first identified key player in UPR and plays essential role in protecting cells against lethal consequences of ER stress.(26)

Recently studies suggested that oxidative stress is one of the mechanism involved in Chop induced cell apoptosis. Our results suggest that iA of **pTC-1** generates cytotoxic reactive oxygen species (ROS, Fig. 4C) in the cell cytoplasm, agreeing with the report that prolonged ER stress hyperoxidizes the ER lumen, resulting in H_2O_2 leakage into the cytoplasm and inducing ROS generation in the cytoplasm.(26) The oxidation environment of ER lumen is induced by Ero1α (Fig. 4A), which hyperoxidizes the ER and promotes cell death. Similar to IRE1α, another branch of UPR is the activation of PERK,(29,30) which is the major protein for attenuating of mRNA translation under ER stress and preventing newly synthesized protein influx into already stressed ER lumen. Our result indicates that PERK activity slightly increases at first 12 h and decreases by 24 h.

Calnexin is another molecular chaperone of ER, which plays an essential role for assisting membrane protein folding. Recent studies demonstrated that the expression levels of calnexin and its association with Bap31 partially contribute cancer cell resistance to apoptosis induced by ER stress.(31) Being treated with **pTC-1**, the expression level of calnexin slightly decreases in A2780cis cells and significantly decreases in HeLa cells. In the A2780cis cells treated with **pTC-1** for 24 h, we also found an additional band of calnexin, the product from the calnexin cleaved by caspase-3 or caspase-7. This result agrees with the report that calnexin is cleaved during apoptosis, as well as under ER stress.(32) Together with expression levels of these ER markers under normal conditions (Figure S9), these results suggest ER stress, induced by **pTC-1**, as one of the mechanism contributing cell death.

Inactivating Src /Akt signaling pathway

Src family kinases (SFKs) play crucial roles in the tumor development, including cell proliferation, survive, invasion, migration, adhesion, and angiogenesis.(33) In fact, most of tumor tissues overexpress or maintain high activation of SFKs.(34) Because of the crucial role of Src in many intracellular signaling processes and in cancer progression, inhibitors of SFKs are currently being developed and undergoing clinical testing.(35) It is also known that Src overexpresses in ovarian cancer cells and interacts with transmembrane receptor tyrosine kinases (RTKs) at the cell membrane.(36) Thus, **pTC-1** should affect the expression of Src in A2780cis cells because iA of **pTC-1** occurs at cell membrane (Figure S5).

We used immunofluorescence to determine the effect of **pTC-1** on the expression of Src. The results (Figure 5A and B) indicate that the expression level of phospho-Src decreases upon the treatment of **pTC-1**, evidenced by the weaker fluorescence than that in the untreated A2780cis cells. Epidermal growth factor receptor (EGFR) is another protein that interacts with Src. Being phosphorylated by Src, EGFR forms complex with Src, which is important for tumorigenesis.(37) Comparing with untreated A2780cis cells, our results show more fluorescence on cell surface (Figure S10), indicating that **pTC-1** changes the distribution of EGFR. Moreover, the expression levels of phospho-Akt (pAkt) and stress activated protein kinase/c-Jun N-terminal kinase (SAPK/JNK), the downstream survival signals of Src, decrease after the treatment of **pTC-1** (Figure 5C, D and E). These results, together, suggest that Src signaling pathway involves in the cell death induced by **pTC-1**. Interestingly, the expression level of JNK also responds to ROS level in cells, which is

mediated by IRE1α (Scheme 1 and Figure 4A). This observation indicates that iA of **pTC-1** results in cross-talks between different cell signaling pathways.

Augmenting anticancer efficiency of TRAIL inducer and doxorubicin

Since **pTC-1** induces the expression of DR5, the receptor of tumor necrosis factor (TNF)-related apoptosis-inducing ligand (TRAIL), we expected that **pTC-1** would increase the cytotoxicity of TRAIL inducers or cognate ligand. We select representative TRAIL inducers, TIC10(38), and soluble cognate ligand, human Apo2L/TRAIL(39), which exhibit potent anticancer efficiency in preclinical trials. Our results indicate that **pTC-1**, with little cytotoxicity at low concentration (8 μM), boosts the cytotoxicity of TIC10 and ApoL/TRAIL (Figure 5F). Moreover, combination of **pTC-1** with doxorubicin, a drug with capacity of sensitizing tumor cells to TRAIL-mediated apoptosis(40), kills A2780cis cells effectively (100 nM of doxorubicin). These results suggest the promise of **pTC-1** in combining with clinical drugs for cancer therapy.

Cell death via the caspase cascade

To investigate the intrinsic signaling pathways involved in cell death induced by **pTC-1**, we characterized the changes of the caspase cascade since our previous results indicated that pan-caspase inhibitor z-VAD and PARP inhibitor PJ34 partially rescue cells treated by **pTC-1**.(15) As shown in figure 6A and B, the expression levels of proteolytically-cleaved caspase-3, caspase-8, and poly (ADP-ribose) polymerase (PARP) increase in both A2780cis and HeLa cells, confirming that **pTC-1** activates caspase-3 and caspase-8. The activation of these proteins are also measured by ELISA kit in a time dependent experiment. Caspase-3 and active PARP increase after A2780cis treated with **pTC-1** for 12 h, more than four times than those in the untreated cells. The expression level of phsopho-Bad increases slightly, and Bad remains almost constant with the treatment of **pTC-1**. A2780cis cells treated with **pTC-1** express a high level of phosphorylated p53 and p53 over the extended incubation time, while the expression level of phosphorylated p53 slightly changes in HeLa cells.

Bio-distribution and inhibition effect of pTC-1/TC-1 on tumor growth *in vivo*

To investigate the distribution of the assembling cholesterol derivatives in tumor bearing murine model, we synthesized four analogues of **pTC-1** that had an additional tyrosine residue for radiolabelling (by ^{125}I(41)) (Figure 7A). Specifically, we connect L or D enantiomer of tyrosine at N terminal of **pTC-1** to form cho-$_p$yY or cho-$_p$yy (cho = cholesterol, $_p$y = D-phosphotyrosine, Y = tyrosine, and y = D-tyrosine). We also put one additional L- or D-tyrosine between cholesterol and D-phosphotyrosine, which results in cho-Y$_p$y and cho-y$_p$y, to examine the influence of indirect conjugation of cholesterol and phosphotyrosine on the cytotoxicity of the assemblies of cholesterols against A2780cis cells. The IC_{50} values of cho-$_p$yY, cho-$_p$yy, cho-Y$_p$y, and cho-y$_p$y against A2780cis cells are 45, 15, 17 and 23 μM (Figure 7B and S11), respectively, indicating that addition of tyrosine to **pTC-1** slightly lowers the cytotoxicity.

After reacting ^{125}I with the tyrosine on each analogue and purifying them by HPLC, we use tumor bearing nude mice to evaluate the distribution of each of these four analogues. The results of noninvasive Gamma camera images (Figure 7C to 7F) indicate that the radioactive

signals are enriched in the mouse abdomen areas and the signals decrease little with extension of time, even after injection of these analogues for 96 h (Figure S12). To reveal the detail distribution of each analogue, we quantify the amounts of the **pTC-1** analogs in the main organs of mice by a Gamma counter in a time-dependent manner. The results (Figure 7G to J) indicate that the four compounds are mainly accumulated in liver, followed by blood, spleen, lung, and other organs. With time increasing, the radioactive signals of four analogues decrease to some extent in heart, spleen, lung, kidney, and blood.

The radioactive signals of the four analogues are different in liver. Specifically, in reference with the signal intensities at 1 h, radioactive signals of cho-$_p$yY decrease to 67.9% at 12 h post injection, while the radioactive signals of cho-$_p$yy increase a little at first 6 h and decrease to 84.8% at 12 h. In contrast, the radioactive signals of cho-Y$_p$y and cho-y$_p$y remain almost the same at 1 h and 12 h. The radioactive signals of the four analogues maintain almost constant during tested time in large intestine and brain. Notably, the radioactive signals of cho-$_p$yy and cho-Y$_p$y increase a little in the tumor sites over time, agreeing with that these two compounds potently inhibit A2780cis (Figure 7B).

We then evaluate the efficacy of **pTC-1** for inhibiting tumor growth in an A2780cis bearing nude mice model. After the volume of A2780cis tumor reaches about 50 mm^3, three dosages (1.5, 10 and 25 mg/kg) of **pTC-1** are intraperitoneally injected to the mice. As shown in Figure 7K, **pTC-1** efficiently inhibits the tumor growth in a dose dependent manner at the first 6 days and delays the tumor growth in the following 6 days. Moreover, the results of tumor weights also are consistent with the growth curve of tumors (Figure 7M and N) in mice. These results indicate that **pTC-1** inhibits the growth of the A2780cis tumors moderately. Meanwhile, we also monitored the weight changes of the mice. Our results indicate the mice treated with **pTC-1** at these three dosages have no obvious body weight loss, suggesting good in vivo compatibility of **pTC-1**.

Discussion

This work provides molecular and cellular details of the assemblies of small molecule in vitro and establishes antitumor activity of the assemblies against platinum-resistant tumors in vivo. Cell based screening indicate that iA of **pTC-1** have more potent activity against ovarian cancer cells, which is independent to the cholesterol levels in different cell types, indicating the importance of enzymatic reaction for the cytotoxicity of iA. The less cytotoxicity of **pTC-1** on HepG2 cells suggests that in vivo liver toxicity of **pTC-1** should be low since HepG2 often acts as a model cell of hepatocyte. Our preliminary results of acquired resistance experiment indicate that **pTC-1**, averting resistance, likely would minimize acquired drug resistance. The change of actin filaments in both A2780cis and HeLa cells with the increment of time, imply that iA of **pTC-1** gradually disrupts the dynamics of actin filaments, which contributes to the cell death induced by **pTC-1**. Moreover, the changes of the morphology of mitochondria during cell death implies that the cell death involves a mitochondria dependent apoptosis.(42)

Interestingly, after the treatment with **pTC-1** for 24 h, the band of TNF-R2 disappears in both A2780cis and HeLa cells, likely is resulted from the degradation by the ubiquitin

proteasome pathway. Unlike TNF-R1 that contains an intracellular death domain and can activate apoptotic pathways, TNF-R2 mediates cell survive and proliferation.(43) Recent finding also revealed TNF-R2 could be a target for cancer immunotherapy(44,45) and its up-regulation could be the reason for drug resistance.(46,47) Although the reason for degradation of TNF-R2 in both A2780cis and HeLa cells remains to be addressed in future studies, the abnormal expression of TNF-R2 may contribute to the lack of acquired resistance of **pTC-1** in A2780. The results of time-dependent Western blot of death receptors clearly indicate that the signaling induced by **pTC-1** leads to the formation of death inducing signaling complex (DISC) through the death receptors, including CD95, DR3, DR5, and TNF-R1, which further activate caspase cascade and induce cell death.

Although PERK plays an important role for adapting ER stress to cell survival during the unfolded protein response, the estimated half-life of PERK is 13 h and it is impossible that much of the PERK expressed at one time in cells during ER stress. Moreover, under prolonged ER stress, inactivity of PERK leads to increased activity of other ER stress pathway, for example, the parallel ER stress pathways of IRE1 couple to JNKs may play key role for inducing cell death, agreeing with a previous report.(48,49) Collectively, our results clearly implies that ER stress plays crucial role in **pTC-1** induced cancer cell death. That is, the ER stress activates both IRE1 and PERK branch of UPR, resulting in the activation of Bip, DR5, and Ero1α to promoting CHOP expression. The cross talks of different signaling pathways together activate caspase cascade and the related extrinsic cell death pathway, thus inducing cell death.

Finally, we use tumor bearing murine model to see the detail distribution of pTC-1. The results indicate that **pTC-1** have longer blood circulation as compared with the reported self-assembling peptides, which degrade completely after 12 h in vivo,(50) this result implies that doping cholesterol may provide an alternative strategy for enhancing blood circulation of therapeutic peptides. We also conduct the therapeutic activity of **pTC-1** against cisplatin resistance tumor model. The in vivo studies demonstrate the well biocompatibility and anti-tumor efficiency of **pTC-1**. Although anti-tumor efficiency of **pTC-1** remains to be improved, its unprecedented ability to avert drug resistance (Figure S1) and to enhance the efficacy of TIC10 or TRAIL (Figure 5) warrants further exploration of this polypharmaceutical agent.

In summary, using an array of biochemical methods, we examined the mechanism of iA of **pTC-1** that induced cancer cell death selectively. Although dying cells can release contents to induce immunogenic cell death (ICD) by relatively restricted set of stimuli, **pTC-1** is unlikely to initiate ICD since it causes cell death via apoptosis. This study provides a comprehensive understanding of the signal pathways (Scheme 1) involved in the cancer cell death induced by **pTC-1** via enzymatically forming supramolecular assemblies.(15) As a multifaceted strategy induce cell death, iA minimizes acquired drug resistance with continuous treatment of cancer cells with **pTC-1**. Unlike traditional therapies which focus on targeting one specific protein or signaling pathway, this study not only highlights the advantage of therapeutic effect of iA for addressing drug resistance, but also provides a prospective method for improving the efficiency of clinical drugs. Because of a network of multiple proteins involved in one disease, the kinetics and systemic responses of cells to

instructed assemblies offer new understanding on the dynamic changes of live system to molecular processes. Further exploration of the iA of small molecules as a molecular process promises novel therapeutics for cancer therapy.

Supplementary Material

Refer to Web version on PubMed Central for supplementary material.

Acknowledgments

This work was partially supported by NIH (CA142746), NSF (DMR-1420382) and W. M. Keck Foundation. ZF thanks the Dean's fellowship and NIH (F99CA234746). We thank Dr. D. R. Green for providing 2H18 HeLa cells.

References

1. Stratton MR, Campbell PJ, Futreal PA. The cancer genome. Nature 2009;458:719–24 [PubMed: 19360079]
2. Hudson TJ, Anderson W, Aretz A, Barker AD, Bell C, Bernabé RR, et al. International network of cancer genome projects. Nature 2010;464:993–8 [PubMed: 20393554]
3. Parsons DW, Jones S, Zhang X, Lin JC-H, Leary RJ, Angenendt P, et al. An integrated genomic analysis of human glioblastoma multiforme. Science 2008;321:1807–12 [PubMed: 18772396]
4. Avendaño C, Menendez JC. Medicinal chemistry of anticancer drugs. Elsevier; 2015.
5. Sharma P, Hu-Lieskovan S, Wargo JA, Ribas A. Primary, adaptive, and acquired resistance to cancer immunotherapy. Cell 2017;168:707–23 [PubMed: 28187290]
6. Hopkins AL. Network pharmacology: the next paradigm in drug discovery. Nat Chem Biol 2008;4:682–90 [PubMed: 18936753]
7. Simons K, Ikonen E. How cells handle cholesterol. Science 2000;290:1721–6 [PubMed: 11099405]
8. Simons K, Ikonen E. Functional rafts in cell membranes. nature 1997;387:569–72 [PubMed: 9177342]
9. Yang W, Bai Y, Xiong Y, Zhang J, Chen S, Zheng X, et al. Potentiating the antitumour response of CD8+ T cells by modulating cholesterol metabolism. Nature 2016;531:651–5 [PubMed: 26982734]
10. Wang H, Feng Z, Wang Y, Zhou R, Yang Z, Xu B. Integrating Enzymatic Self-Assembly and Mitochondria Targeting for Selectively Killing Cancer Cells without Acquired Drug Resistance. Journal of the American Chemical Society 2016;138:16046–55 [PubMed: 27960313]
11. Feng Z, Wang H, Zhou R, Li J, Xu B. Enzyme-Instructed Assembly and Disassembly Processes for Targeting Downregulation in Cancer Cells. Journal of the American Chemical Society 2017;139:3950–3 [PubMed: 28257192]
12. Gao Y, Shi J, Yuan D, Xu B. Imaging enzyme-triggered self-assembly of small molecules inside live cells. Nature communications 2012;3:1033
13. Fonta C, Négyessy L. Neuronal Tissue-Nonspecific Alkaline Phosphatase (TNAP). Springer; 2015.
14. Kuang Y, Shi J, Li J, Yuan D, Alberti KA, Xu Q, et al. Pericellular hydrogel/nanonets inhibit cancer cells. Angewandte Chemie International Edition 2014;53:8104–7 [PubMed: 24820524]
15. Wang H, Feng Z, Wu D, Fritzsching KJ, Rigney M, Zhou J, et al. Enzyme-regulated supramolecular assemblies of cholesterol conjugates against drug-resistant ovarian cancer cells. Journal of the American Chemical Society 2016;138:10758–61 [PubMed: 27529637]
16. Nikounezhad N, Nakhjavani M, Shirazi FH. Generation of cisplatin-resistant ovarian cancer cell lines. Iranian Journal of Pharmaceutical Sciences 2016;12:11–20
17. Boldogh IR, Pon LA. Interactions of mitochondria with the actin cytoskeleton. Biochimica et Biophysica Acta (BBA)-Molecular Cell Research 2006;1763:450–62 [PubMed: 16624426]
18. Tsai JC, Wu CL, Chien HF, Chen CT. Reorganization of cytoskeleton induced by 5-aminolevulinic acid-mediated photodynamic therapy and its correlation with mitochondrial dysfunction. Lasers in surgery and medicine 2005;36:398–408 [PubMed: 15856508]

19. Estaquier J, Arnoult D. Inhibiting Drp1-mediated mitochondrial fission selectively prevents the release of cytochrome c during apoptosis. Cell Death & Differentiation 2007;14:1086–94 [PubMed: 17332775]
20. Goldstein JC, Waterhouse NJ, Juin P, Evan GI, Green DR. The coordinate release of cytochrome c during apoptosis is rapid, complete and kinetically invariant. Nature cell biology 2000;2:156 [PubMed: 10707086]
21. Koh CHV, Cheung NS. Cellular mechanism of U18666A-mediated apoptosis in cultured murine cortical neurons: bridging Niemann–Pick disease type C and Alzheimer's disease. Cellular signalling 2006;18:1844–53 [PubMed: 16797161]
22. Ashkenazi A, Salvesen G. Regulated cell death: signaling and mechanisms. Annual review of cell and developmental biology 2014;30:337–56
23. Shatnyeva OM, Kubarenko AV, Weber CE, Pappa A, Schwartz-Albiez R, Weber AN, et al. Modulation of the CD95-induced apoptosis: the role of CD95 N-glycosylation. PLoS One 2011;6:e19927 [PubMed: 21625644]
24. Lu M, Lawrence DA, Marsters S, Acosta-Alvear D, Kimmig P, Mendez AS, et al. Opposing unfolded-protein-response signals converge on death receptor 5 to control apoptosis. Science 2014;345:98–101 [PubMed: 24994655]
25. Yamaguchi H, Wang H-G. CHOP is involved in endoplasmic reticulum stress-induced apoptosis by enhancing DR5 expression in human carcinoma cells. Journal of Biological Chemistry 2004;279:45495–502 [PubMed: 15322075]
26. Tabas I, Ron D. Integrating the mechanisms of apoptosis induced by endoplasmic reticulum stress. Nature cell biology 2011;13:184 [PubMed: 21364565]
27. Zlotorynski E Apoptosis: DR5 unfolds ER stress. Nature Reviews Molecular Cell Biology 2014;15:498
28. Feng B, Yao PM, Li Y, Devlin CM, Zhang D, Harding HP, et al. The endoplasmic reticulum is the site of cholesterol-induced cytotoxicity in macrophages. Nature cell biology 2003;5:781 [PubMed: 12907943]
29. Ron D, Walter P. Signal integration in the endoplasmic reticulum unfolded protein response. Nature reviews Molecular cell biology 2007;8:519 [PubMed: 17565364]
30. Harding HP, Zhang Y, Ron D. Protein translation and folding are coupled by an endoplasmic-reticulum-resident kinase. Nature 1999;397:271 [PubMed: 9930704]
31. Delom F, Emadali A, Cocolakis E, Lebrun J, Nantel A, Chevet E. Calnexin-dependent regulation of tunicamycin-induced apoptosis in breast carcinoma MCF-7 cells. Cell death and differentiation 2007;14:586 [PubMed: 16858427]
32. Takizawa T, Tatematsu C, Watanabe K, Kato K, Nakanishi Y. Cleavage of calnexin caused by apoptotic stimuli: implication for the regulation of apoptosis. Journal of biochemistry 2004;136:399–405 [PubMed: 15598898]
33. Zhang S, Yu D. Targeting Src family kinases in anti-cancer therapies: turning promise into triumph. Trends in pharmacological sciences 2012;33:122–8 [PubMed: 22153719]
34. Kim LC, Song L, Haura EB. Src kinases as therapeutic targets for cancer. Nature reviews Clinical oncology 2009;6:587
35. Mayer EL, Krop IE. Advances in targeting SRC in the treatment of breast cancer and other solid malignancies. Clinical Cancer Research 2010;16:3526–32 [PubMed: 20634194]
36. Manek R, Pakzamir E, Mhawech-Fauceglia P, Pejovic T, Sowter H, Gayther SA, et al. Targeting Src in endometriosis-associated ovarian cancer. Oncogenesis 2016;5:e251 [PubMed: 27526105]
37. Chen Z, Oh D, Dubey AK, Yao M, Yang B, Groves JT, et al. EGFR family and Src family kinase interactions: mechanics matters? Current opinion in cell biology 2018;51:97–102 [PubMed: 29289897]
38. Allen JE, Krigsfeld G, Mayes PA, Patel L, Dicker DT, Patel AS, et al. Dual inactivation of Akt and ERK by TIC10 signals Foxo3a nuclear translocation, TRAIL gene induction, and potent antitumor effects. Science translational medicine 2013;5:171ra17-ra17
39. Nair PM, Flores H, Gogineni A, Marsters S, Lawrence DA, Kelley RF, et al. Enhancing the antitumor efficacy of a cell-surface death ligand by covalent membrane display. Proceedings of the National Academy of Sciences 2015;112:5679–84

40. Wang S, Ren W, Liu J, Lahat G, Torres K, Lopez G, et al. TRAIL and doxorubicin combination induces proapoptotic and antiangiogenic effects in soft tissue sarcoma in vivo. Clinical Cancer Research 2010;16:2591–604 [PubMed: 20406839]

41. Buchsbaum DJ, Walker PC, Johnson EA. Distribution of Radiolabeled Alloantibodies in Mice Bearing 3-Methylcholanthrene-induced Sarcomas. Cancer research 1979;39:3363–8 [PubMed: 476667]

42. Frank S, Gaume B, Bergmann-Leitner ES, Leitner WW, Robert EG, Catez F, et al. The role of dynamin-related protein 1, a mediator of mitochondrial fission, in apoptosis. Developmental cell 2001;1:515–25 [PubMed: 11703942]

43. Aggarwal BB. Signalling pathways of the TNF superfamily: a double-edged sword. Nature reviews immunology 2003;3:745

44. Torrey H, Butterworth J, Mera T, Okubo Y, Wang L, Baum D, et al. Targeting TNFR2 with antagonistic antibodies inhibits proliferation of ovarian cancer cells and tumor-associated Tregs. Sci Signal 2017;10:eaaf8608 [PubMed: 28096513]

45. Vanamee ÉS, Faustman DL. TNFR2: A Novel Target for Cancer Immunotherapy. Trends in molecular medicine 2017

46. Zhao T, Li H, Liu Z. Tumor necrosis factor receptor 2 promotes growth of colorectal cancer via the PI3K/AKT signaling pathway. Oncology letters 2017;13:342–6 [PubMed: 28123565]

47. Yang F, Zhao N, Wu N. TNFR2 promotes Adriamycin resistance in breast cancer cells by repairing DNA damage. Molecular medicine reports 2017;16:2962–8 [PubMed: 28677724]

48. Harding HP, Zhang Y, Bertolotti A, Zeng H, Ron D. Perk is essential for translational regulation and cell survival during the unfolded protein response. Molecular cell 2000;5:897–904 [PubMed: 10882126]

49. Bertolotti A, Zhang Y, Hendershot LM, Harding HP, Ron D. Dynamic interaction of BiP and ER stress transducers in the unfolded-protein response. Nature cell biology 2000;2:326 [PubMed: 10854322]

50. Yang C, Chu L, Zhang Y, Shi Y, Liu J, Liu Q, et al. Dynamic biostability, biodistribution, and toxicity of L/D-peptide-based supramolecular nanofibers. ACS applied materials & interfaces 2015;7:2735–44 [PubMed: 25555064]

Implications:

As a multifaceted strategy for controlling cancer cell death, instructed-assembly (iA) minimized acquired resistance of cancer cells, which is a new strategy to amplify the genetic difference between cancer and normal cells and provides a promises for overcoming drug resistance in cancer therapy.

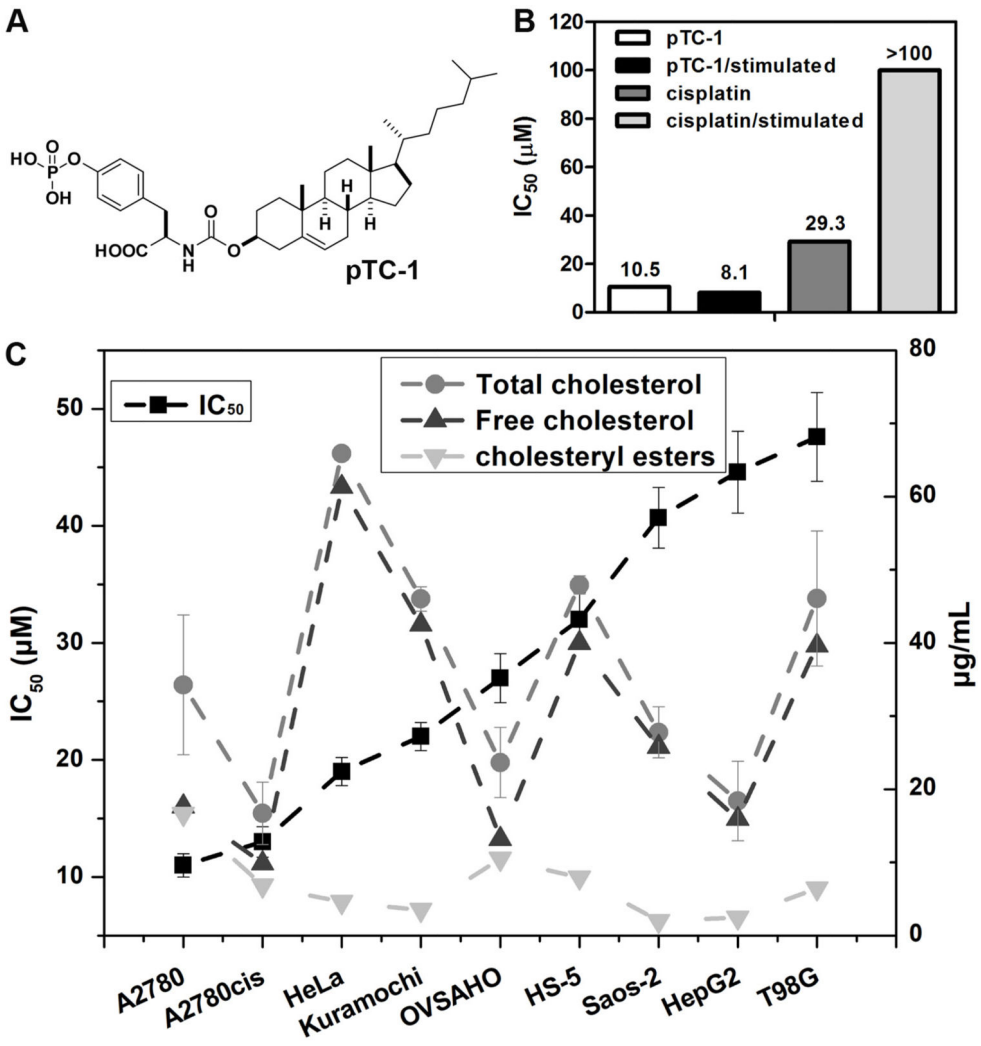

Figure 1.

Cytotoxicity of phosphotyrosine cholesterol (**pTC-1**) and the selective inhibition of multiple cancer cells. (A) Molecular structure of **pTC-1**; (B) 48 h IC_{50} of **pTC-1** against unstimulated A2780 cell line or stimulated A2780 cell line (after five weeks treatment of the precursors with gradually increase concentrations); (C) IC_{50} of **pTC-1** against different cell lines for 48 h and the cholesterol contents of different cell lines.

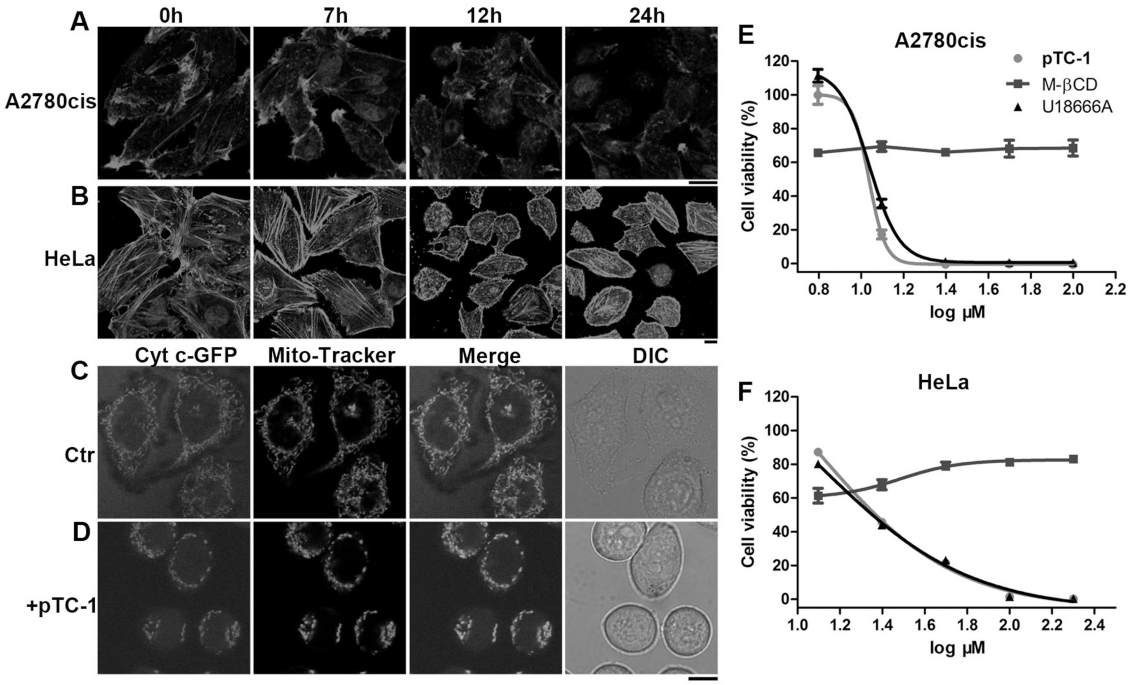

Figure 2.

pTC-1 interacts with cell cytoskeleton and induces mitochondria fission. After incubating **pTC-1** with (A) A2780cis or (B) HeLa cells to reach designated time points, we used Alexa Fluor 633 phalloidin (F-actin) to reveal the changes of actin filaments. The concentration of **pTC-1** is 12.5 μM for A2780cis cell and 25 μM for HeLa cell. (C) and (D) **pTC-1** (25 μM) induced fragmental mitochondria in 2H18 HeLa cells (expressing GFP labeled Cyt c). After treated 2H18 HeLa cells for 22 h by **pTC-1**, we also used Mito-Tracker to stain cellular mitochondria. 48 h cell viability of (E) A2780cis or (F) HeLa without or with addition of M-βCD and U18666A. The concentrations of M-βCD for treating A2780cis and HeLa cells are 5 and 2 mM, respectively. The concentration of U18666A for treating A2780cis and HeLa cell is 1 μg/mL. Scale bar in (A) to (D) is 10 μm.

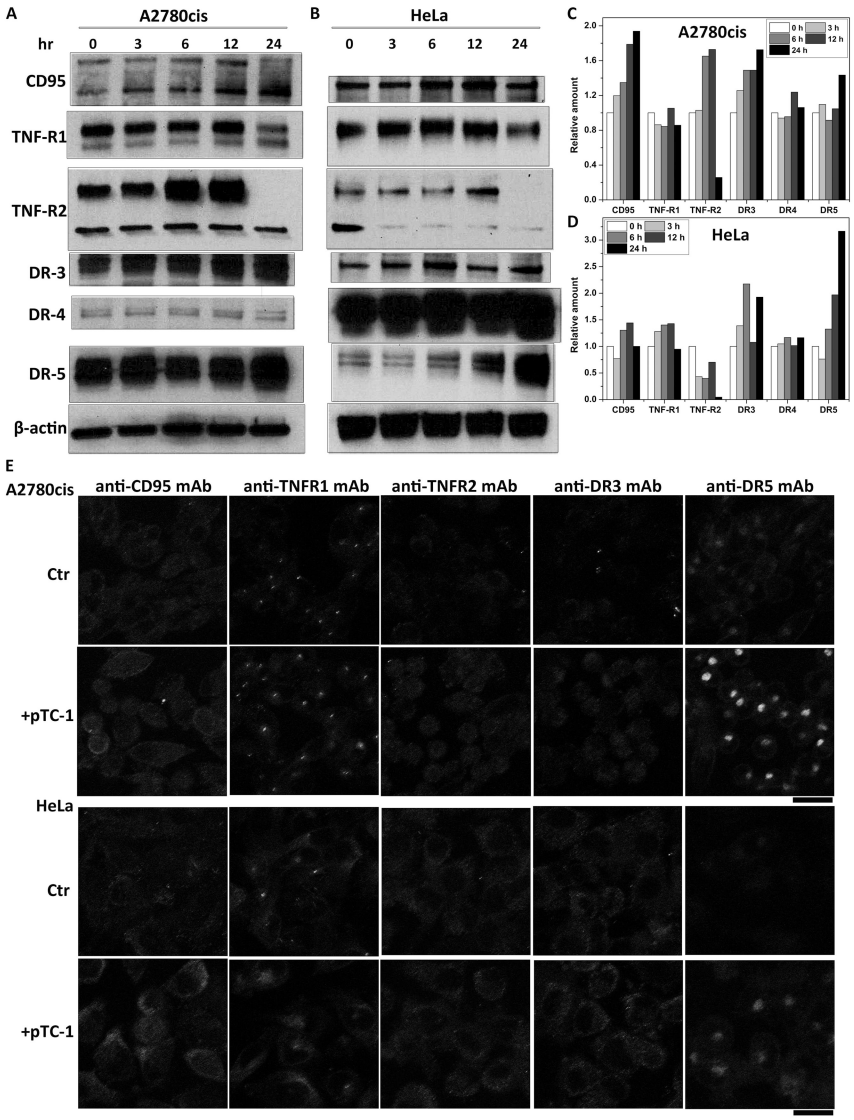

Figure 3.

pTC-1 affects the expression of death receptors. Western blot indicates that the expression level changes of relative amounts of cell death receptors upon the treatment of **pTC-1** (A) A2780cis and (B) HeLa cell lines. The quantification of expression level of cell death receptors from Western blot (C) in A2780cis and (D) HeLa cell lines. (E) Immunofluorescence shows the changes of cell death receptors without or with the treatment of **pTC-1** in A2780cis or HeLa cell lines for 24 h.

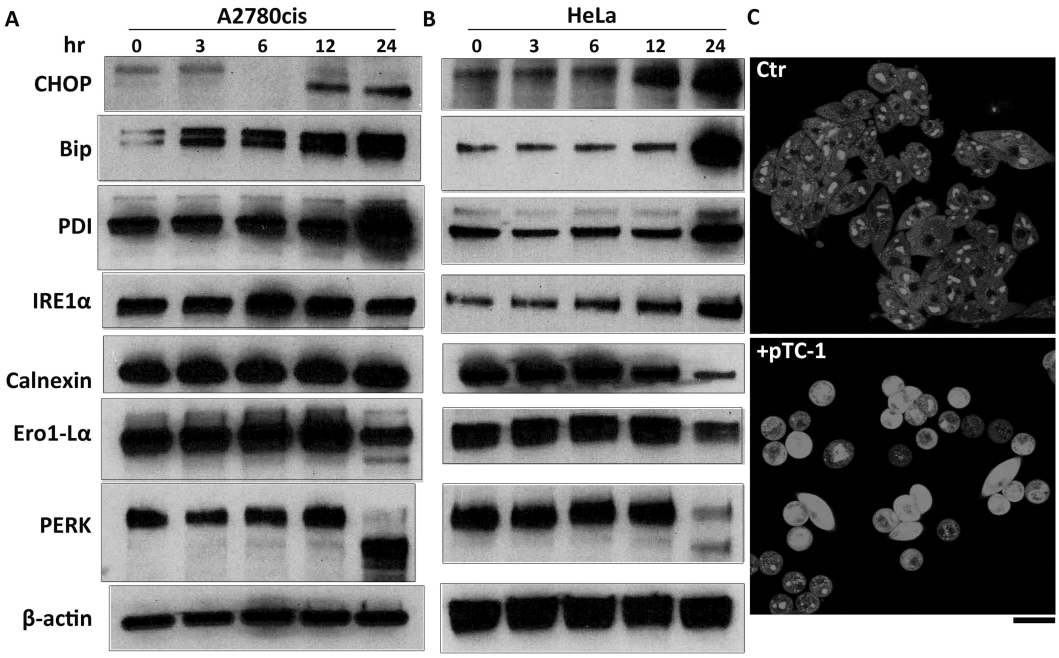

Figure 4.

pTC-1 induces cell apoptosis via ER stress and generates ROS. Western blot indicates the changes of the expression of ER stress markers in (A) A2780cis and (B) HeLa cell lines upon the treatment of **pTC-1**. (C) CLSM images showing the generation of ROS as measured by dehydroethidium (DHE, λex = 543 nm, emission was detected at 575–625 nm) in A2780cis without and with treatment with **pTC-1** (12.5 μM) for 12 h.

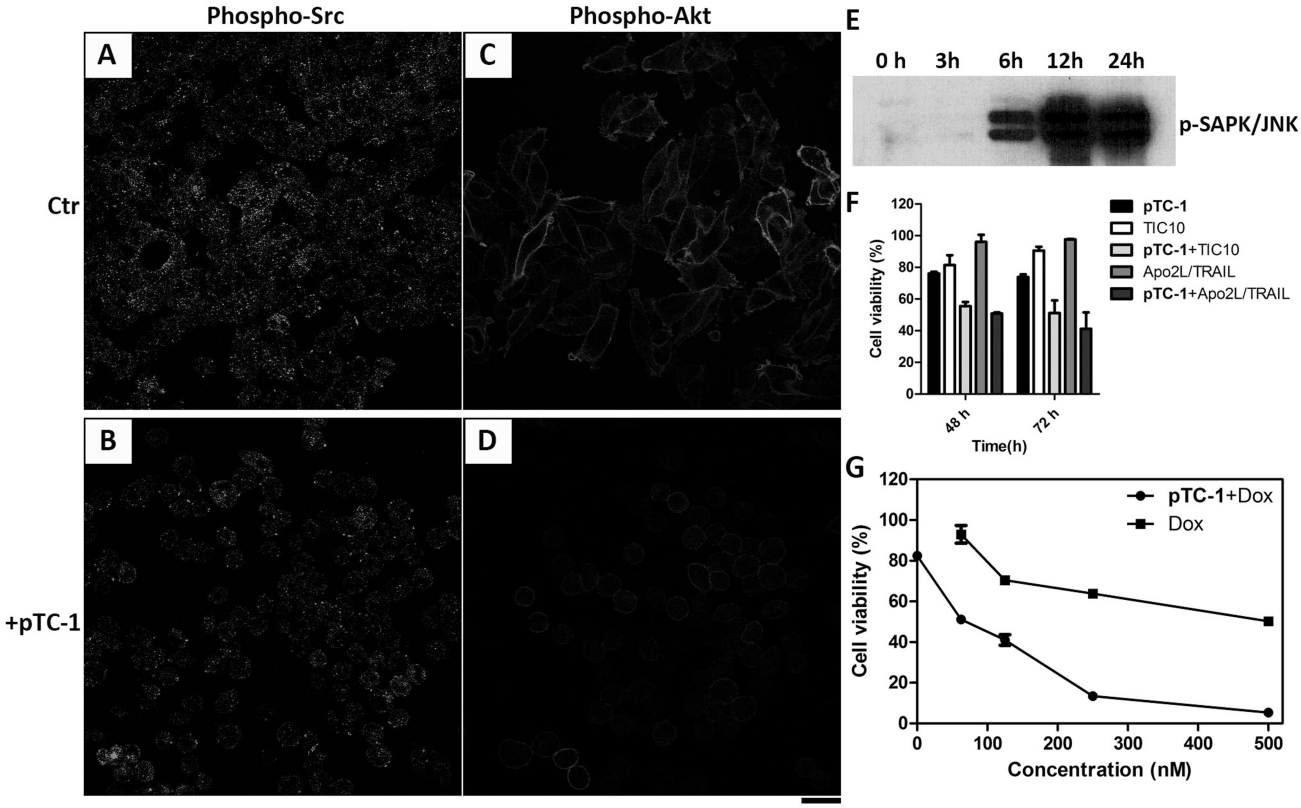

Figure 5.

pTC-1 decreases the expressions of (A, B) Src and (C, D) Akt in A2780cis cell lines after the treatment of **pTC-1** (12.5 μM) for 24 h. Scale bar is 25 μm. (E) Time-dependent Western blot shows the expression levels of p-SAPK/JNK in A2780cis cell lines. **pTC-1** (8 μM) enhances the effect of different anticancer agents: (F) TIC 10 (5 μM) and Apo2L/TRAIL (50 ng/mL) and (G) doxorubicin at different concentrations.

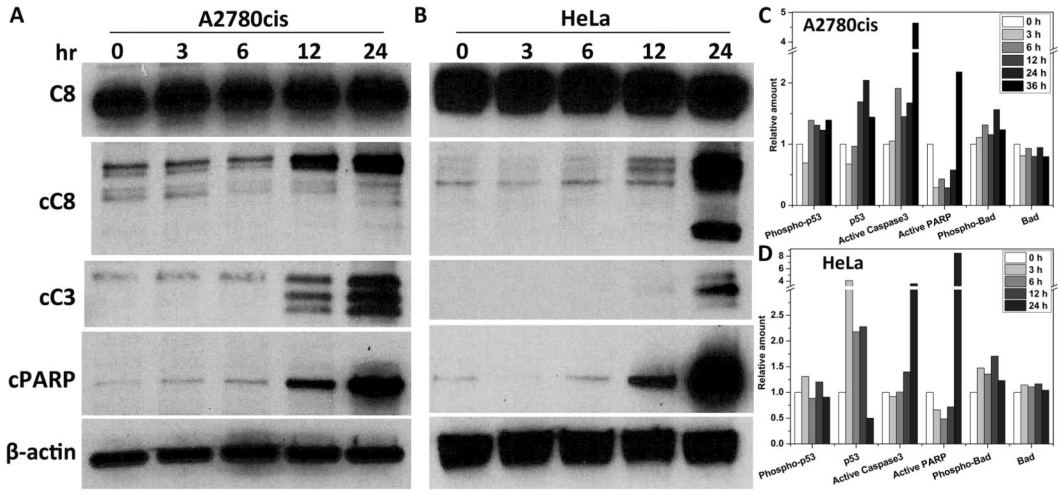

Figure 6.

pTC-1 activates the down-stream apoptotic proteins. Time-dependent Western blot shows the expression levels of C8 (caspase-8), cC8 (cleaved caspase-8), cC3 (cleaved caspase-3) and cPARP (cleaved PARP) in (A) A2780cis and (B) HeLa cell lines. Time-dependent ELISA of activation of apoptotic proteins in (C) A2780cis and (D) HeLa cells treated with **pTC-1**.

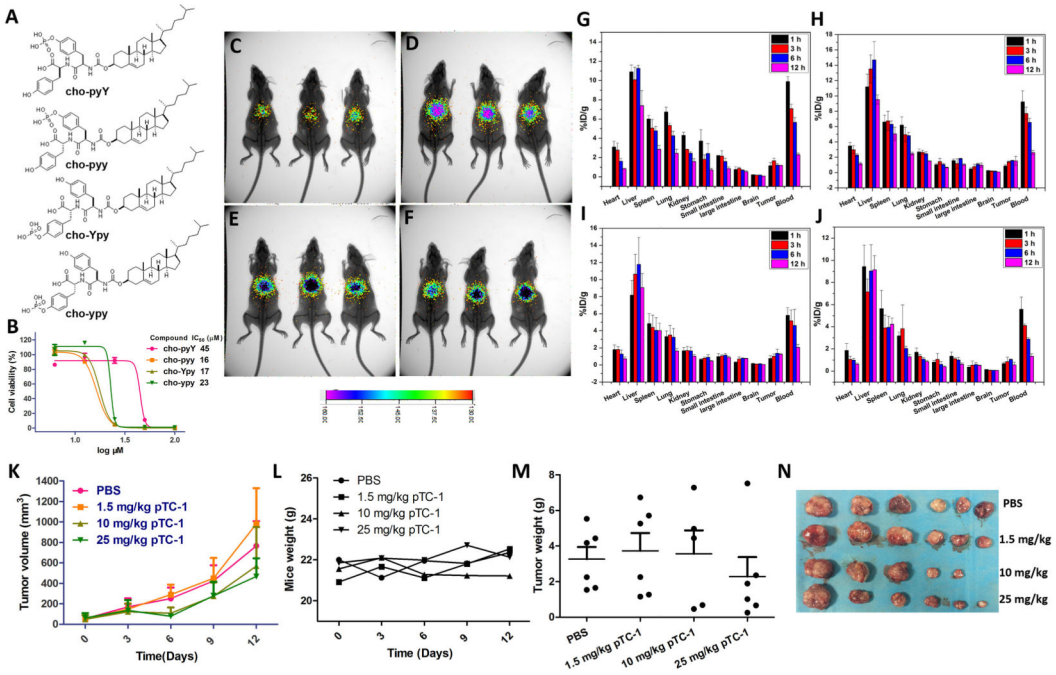

Figure 7.

In vivo distribution and tumor inhibition of the conjugates of cholesterol and tyrosine. (A) Molecular structures of the analogues of **pTC-1**; (B) 48 h cell viability of A2780cis cell lines treated by the analogues of **pTC-1** in (A). (C-F) In vivo noninvasive Gamma camera images of the BALB/c mice after intravenous administration with ^{125}I-labeled different cholesterol derivatives (C: cho-$_p$yY; D: cho-$_p$yy; E: cho-Y$_p$y; F: cho-y$_p$y) for 12 h, respectively. (G-J) Quantitative biodistribution of ^{125}I-labeled cholesterol derivatives. Tissues were harvested and weighted at 1, 3, 6, and 12 h after initial injection of BALB/c mice, respectively. Data (G: cho-$_p$yY; H: cho-$_p$yy; I: cho-Y$_p$y; J: cho-y$_p$y) were presented as percent injected dose per gram (%ID/g) ± standard deviation, n = 3. **pTC-1** inhibits xenografted mouse ovarian cancer tumor (A2780cis) in vivo (n = 6): (K) The changes of tumor volume; (L) the changes of mice weight; (M) tumor weight after grows for 12 days; (N) Optical images of tumors after grows for 12 days.

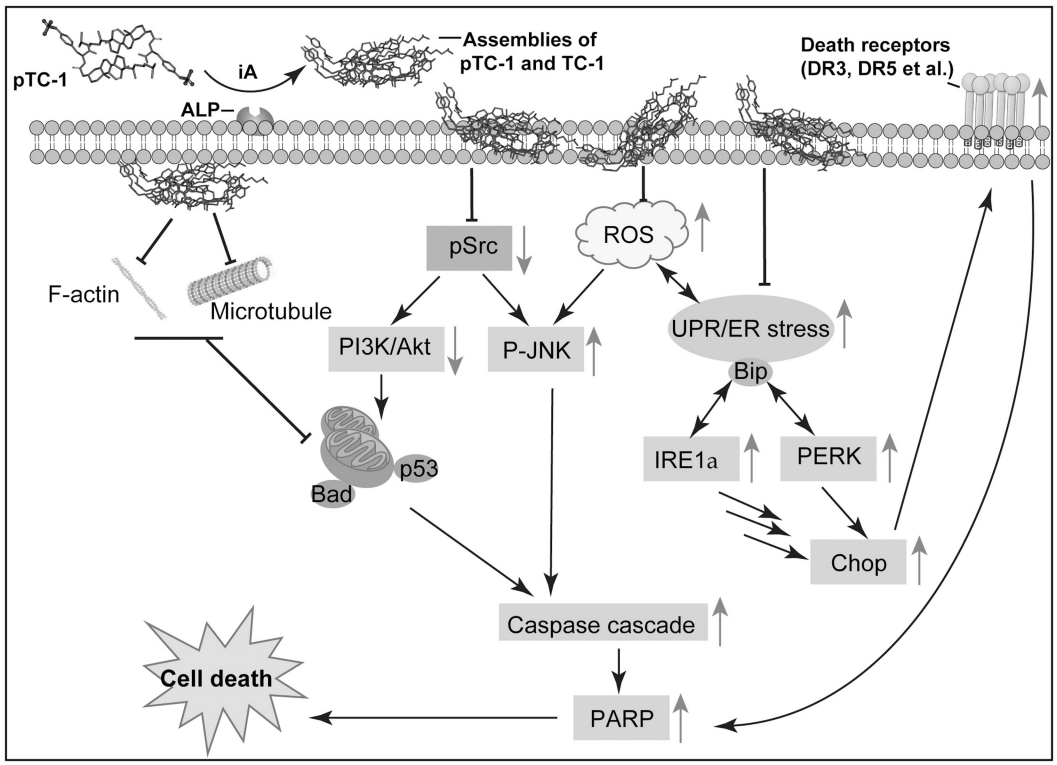

Scheme 1.

Mechanism of the iA of **pTC-1/TC-1** that induces cancer cell death. The up arrow indicates the up-regulation of protein expression and *vice versa*.